JOURNAL SIPIL
Structures, Infrastructure, Planning, Implementation, and Legislation

Analytical Assessment of FRP Confined Circular Reinforced Concrete Sections under Concentric Axial Compression

Hamzah Al Imran[1]*, Fajar Ramdhan Asari[2], & Muhammad Yose[3]
[1]*Universitas Muhammadiyah Makassar, Indonesia , [2]Universitas Putra Indonesia "YPTK" Padang, Indonesia, [3]Universitas Putra Indonesia "YPTK" Padang, Indonesia
*Co e-mail: fajarramdhan@gmail.com[1]

Article Information
Received: September 30, 2026
Revised: October 20, 2026
Online: October 30, 2026

Keywords
FRP Confinement, Circular RC Section, Analytical Comparison, Ideal Axial Capacity, Axial Strain Capacity, Confinement Ratio

ABSTRACT

Purpose: This analytical study compares confinement equations for a 400 mm circular reinforced concrete section with eight D16 bars, assumed CFRP or GFRP wraps, and concrete strengths of 20, 25, and 30 MPa. Methods: Thirty input combinations represent 27 unique conditions. Lam–Teng results are compared with explicitly labeled ACI 440.2R-17 evaluations, including its minimum confinement-ratio criterion. Results: At 25 MPa, two to four CFRP layers increase predicted concrete strength by 45.6–91.3% and ideal section capacity by 36.3–72.6% in the adopted Lam–Teng implementation. The one-layer ratio is 0.069138, below its 0.07 strength-gain threshold; the retained flat-branch idealization gives no strength increase but a higher terminal axial strain. All six one-layer ACI cases are below the 0.08 ratio criterion and are excluded from strengthening-capacity conclusions. For ratio-qualified cases at 25 MPa, ACI strength values are 4.0–6.2% lower. With a peak concrete strain of 0.002, its terminal strain rises from 8.8‰ at two layers to 10.0‰ at three layers and remains capped at four layers. For the matched 25 MPa four-layer input systems, GFRP terminal strain is 13.33% higher than CFRP. Conclusion: This difference is conditional on the assumed material properties. Reproducible calculations and threshold sensitivity are supplied; the study does not establish experimental accuracy, cyclic seismic performance, or an economic optimum.

Keywords: *FRP Confinement, Circular RC Section, Analytical Comparison, Ideal Axial Capacity, Axial Strain Capacity, Confinement Ratio*

INTRODUCTION

Reinforced concrete (RC) columns are the primary vertical load-carrying members of buildings and bridges. Low concrete strength, inadequate transverse reinforcement, deterioration, and increased service loads can motivate structural retrofit. In Indonesia, design provisions for concrete structures are given in SNI 2847:2019 (Badan Standardisasi Nasional [BSN], 2019). This standard provides the structural context; the FRP confinement comparison considered here is based on separate published

DOI: http://doi.org/10.69855/sipil.v2i2.900
Available online at website: https://gpijournal.com/index.php/sipil

This work is licensed under a Creative Commons Attribution 4.0 International license

models and guidance. Wrapping with externally bonded fiber-reinforced polymer (FRP) sheets offers a strengthening option with a relatively small change in section dimensions.

The mechanism is passive confinement. Under axial compression the concrete dilates laterally, the FRP jacket, which is stiff and linear-elastic in the hoop direction, resists this expansion, and the resulting confining pressure raises both the compressive strength and the ultimate strain of the concrete core. Because of this, the behavior of FRP-confined concrete has been the subject of a very large body of experimental and theoretical work. A recent state-of-the-art review focuses on columns that show a stress reduction–recovery response and on design recommendations and model assessment for that behavior (Liao et al., 2023), and unified models for circular and non-circular cross-sections continue to appear (Shayanfar et al., 2022; Shayanfar, Barros, Abedi, & Rezazadeh, 2023; Shayanfar, Barros, & Rezazadeh, 2023; Shayanfar & Barros, 2024).

Recent studies have extended the topic in several directions. Design-oriented models have been formulated for columns that may show post-peak softening followed by hardening, and for a general cross-section (Shayanfar & Barros, 2024; Shayanfar et al., 2024). Large-rupture-strain FRP made of polymers such as PET and PEN has been tested on columns of different sizes, and size-dependent and unified stress–strain models have been proposed (Yuan, Bai, et al., 2022; Yuan, Han, & Bai, 2022). Confinement has also been studied for steel-reinforced high-strength concrete columns (Chen et al., 2020), for rubber concrete columns (Cao et al., 2022), for steel-fiber-reinforced RC columns under eccentric compression (Nematzadeh et al., 2021), and for fire- or heat-damaged columns, including prestressed FRP confinement (Shayanfar, Pereira, & Barros, 2025; Shayanfar, Barros, et al., 2025). These works show that FRP wrapping is versatile, but they also show that the predicted benefit depends on the model used and on the confinement level.

The present study examines how layer count and assumed concrete strength affect the predictions of two specified confinement formulations when geometry and reinforcement are held constant. It also asks whether the low-confinement cases satisfy the strength-gain or applicability criteria used in each formulation. The CFRP and GFRP comparison concerns two assumed material systems selected to have nearly matched confinement pressures; it does not isolate fiber type as a single independent variable. The study is a controlled analytical comparison rather than a new constitutive model or an experimental assessment.

The objectives are (i) to compare confined strength, terminal axial strain, a defined axial strain index, and ideal section capacity; (ii) to examine two assumed FRP systems and unconfined concrete strengths of 20, 25, and 30 MPa; and (iii) to distinguish formula evaluations from the confinement criteria associated with Lam and Teng (2003) and ACI 440.2R-17 (ACI Committee 440, 2017). The contribution is a reproducible numerical comparison with explicit domain labels and a sensitivity check near the adopted threshold. No independent experimental validation is claimed.

METHODS

1. Study design and section

An analytical parametric study was carried out on a circular RC section with diameter D = 400 mm (A_g = 125,663.706 mm^2) and eight D16 longitudinal bars (A_s = 1,608.495 mm^2; reinforcement ratio 1.28%). Longitudinal steel was idealized as elastic–perfectly plastic with f_y = 420 MPa and E_s = 200 GPa. Three unconfined concrete strengths (f'_{co} = 20, 25, and 30 MPa), two assumed FRP systems, and five wrapping levels (n = 0–4) give 30 combinations. Because the two n = 0 controls at each concrete strength are identical, there are 27 unique conditions. Transverse-steel confinement, bar buckling, and cover loss

This work is licensed under a Creative Commons Attribution 4.0 International license

are not represented. Omitting these mechanisms is an idealization, not evidence that the complete response of an existing column is conservatively predicted.

The section is subjected to uniform concentric axial compression, with fibers oriented in the hoop direction and an ideal full wrap. The terminal condition assumes an effective hoop rupture strain; overlap adequacy and bond failure are not independently evaluated. Member height, effective length, and stability are outside the model, so no physical-column slenderness classification is inferred from the diameter. The circular geometry permits unit shape factors for this comparison. The concrete axial strain and the FRP hoop strain are distinct quantities.

2. Material properties

The numerical input properties are summarized in Table 1. These are assumed parameter sets, not certified commercial products or coupon-test results. The two sets were selected to give nearly matched per-layer pressure at the adopted effective hoop strain: 1.72845 MPa for CFRP and 1.700754 MPa for GFRP with an efficiency factor of 0.60. Their membrane stiffnesses $E_f\ t_f$ are 38,410 and 25,769 N/mm, respectively. Thickness, modulus, and rupture strain therefore vary together. No environmental reduction or material variability is modeled; consistent product-specific property bases would be required for a physical strengthening design.

Table 1. Input parameters of the analytical study

Parameter	Symbol	Value
Column diameter	D	400 mm
Gross section area	A_g	125,663.706 mm^2
Longitudinal reinforcement	8D16 (A_s = 1,608.495 mm^2)	ρ_g = 1.28%
Steel yield strength / modulus	f_y / E_s	420 MPa / 200 GPa
Unconfined concrete strength	f'_{co}	20, 25, 30 MPa
Concrete elastic modulus	E_c	4,700$\sqrt{f'_{co}}$ (MPa)
Strain at peak (unconfined)	ε_{co}	0.002
CFRP: modulus / ply thickness / rupture strain	E_f / t_f / ε_{fu}	230 GPa / 0.167 mm / 1.50 %
GFRP: modulus / ply thickness / rupture strain	E_f / t_f / ε_{fu}	73 GPa / 0.353 mm / 2.20 %
Number of layers	n	0 (control), 1, 2, 3, 4

3. Confinement models

The lateral confining pressure provided by a circular FRP jacket at hoop rupture is

$$f_l = \frac{2E_f n t_f \varepsilon_{h,rup}}{D} \quad (1)$$

In Eq. (1), E_f is the hoop-direction modulus, n the layer count, t_f the assumed per-layer thickness, and $\varepsilon_{h,rup}$ the effective hoop rupture strain. The Lam–Teng comparison adopts $\varepsilon_{h,rup}$ = 0.60 ε_{fu} as a scenario assumption. ACI Committee 440 (2017) reports a mean efficiency near 0.586 from the cited calibration;

This work is licensed under a Creative Commons Attribution 4.0 International license
Structures, Infrastructure, Planning, Implementation, and Legislation (SIPIL)
Vol. 2, No. 2, October 2026

0.60 is not a universal material constant. The ACI expression uses $\varepsilon_{fe} = 0.55\ \varepsilon_{fu}$. Separate pressures are calculated for the two expressions. Sensitivity to the adopted Lam–Teng factor is reported in the Discussion (second sub-section, "Domain checks and parameter sensitivity").

Lam and Teng model. The confined strength and ultimate strain are

$$\frac{f'_{cc}}{f'_{co}} = 1 + 3.3\left(\frac{f_l}{f'_{co}}\right) \text{ for } \frac{f_l}{f'_{co}} \geq 0.07; \quad f'_{cc} = f'_{co} \text{ otherwise} \tag{2}$$

$$\frac{\varepsilon_{cu}}{\varepsilon_{co}} = 1.75 + 12\left(\frac{f_l}{f'_{co}}\right)\left(\frac{\varepsilon_{h,rup}}{\varepsilon_{co}}\right)^{0.45} \tag{3}$$

The strength equation uses the 0.07 branch criterion. For cases below this value, the implementation sets confined strength equal to unconfined strength and retains Eq. (3) as an algebraic terminal-strain estimate. This extension, with a flat second branch, does not model low-confinement softening or stress recovery. The limitations of the original formulation and later refinements are discussed by Teng et al. (2009). The adopted stress–strain relation has a parabolic first branch and a linear second branch:

$$\sigma_c = E_c\varepsilon - \frac{(E_c - E_2)^2\varepsilon^2}{4f'_{co}} \text{ for } 0 \leq \varepsilon \leq \varepsilon_t \tag{4}$$

$$\sigma_c = f'_{co} + E_2\varepsilon \text{ for } \varepsilon_t \leq \varepsilon \leq \varepsilon_{cu} \tag{5}$$

with $E_2 = (f'_{cc} - f'_{co})/\varepsilon_{cu}$ and $\varepsilon_t = 2f'_{co}/(E_c - E_2)$.

ACI 440.2R-17. The strength expression is $f'_{cc} = f'_{co} + \psi_f\, 3.3\, \kappa_a f_l$, where $\psi_f = 0.95$ and $\kappa_a = 1.0$ for a circular section. Its pressure is calculated using $\varepsilon_{fe} = 0.55\ \varepsilon_{fu}$. The ratio f_l/f'_{co} must be at least 0.08 for the confinement criterion examined here (ACI Committee 440, 2,017, Section 12.1). Results below that ratio are explicitly labeled algebraic evaluations and excluded from strengthening-capacity conclusions. Passing this ratio alone does not establish full design compliance. The terminal strain expression is

$$\varepsilon_{ccu} = \varepsilon'_c\left[1.5 + 12\kappa_b\left(\frac{f_l}{f'_{co}}\right)\left(\frac{\varepsilon_{fe}}{\varepsilon'_c}\right)^{0.45}\right] \leq 0.01 \tag{6}$$

The main comparison adopts $\varepsilon'_c = 0.002$, which is permitted in the notation of ACI 440.2R-17, with $\kappa_b = 1.0$. This replaces the earlier choice $\varepsilon'_c = 1.71\, f'_{co}/E_c$; that choice is retained only in the supplementary numerical comparison. The ACI strain values in Table 3 have consequently been recalculated. The 2,017 edition is used as a fixed historical reference, rather than as a statement of compliance with later editions. The stress curves in Figures 2 and 4 use the stated Lam–Teng implementation.

4. Ideal section axial response

The ideal concentric section-capacity index P_0 is calculated from the confined concrete strength and the longitudinal-steel yield contribution:

$$P_0 = 0.85f'_{cc}(A_g - A_s) + f_y A_s \tag{7}$$

For the control, confined strength equals unconfined strength. At axial strain ε, $P(\varepsilon) = 0.85\ \sigma_c(\varepsilon)(A_g - A_s) + \min(E_s\varepsilon, f_y) A_s$. The control curve is explicitly defined as $\sigma_c = f'_{co}\,[2x - x^2]$ for $x = \varepsilon/0.002 \leq 1$ and $\sigma_c = f'_{co}$ from $\varepsilon = 0.002$ to 0.003. Its initial modulus is $2f'_{co}/0.002$, which differs from the assumed $E_c = 4{,}700\sqrt{f'_{co}}$ used in the wrapped curves. The control is a separate chosen idealization. Neither P_0 nor $P(\varepsilon)$ includes a member maximum-strength factor or a final strength-reduction factor; ψ_f remains included in the ACI concrete expression. These outputs are section comparisons, not complete design strengths.

The axial strain index is defined as $\varepsilon_{cu}/0.002$. Monotonic strain energy density W is the integral of concrete axial stress with respect to axial strain, from zero to ε_{cu}, converted from MPa to kJ/m^3 by multiplying by 1,000. W is energy per material volume under the specified monotonic curve, not hysteretic dissipation. The supplementary script integrates each branch analytically and checks trapezoidal estimates with 1,000 and 2,000 intervals, including branch transitions. Across 27 unique

This work is licensed under a Creative Commons Attribution 4.0 International license

conditions, the absolute numerical integration error is below 0.01 kJ/m^3. Domain decisions and geometric areas use full precision; only displayed values are rounded.

RESULTS

1. Confining pressure and confined strength

Table 2(a) gives the separate pressures, unrounded decision ratios, and ACI ratio status for CFRP at f'_{co} = 25 MPa. Table 2(b) gives the corresponding strength and ideal section-capacity indices. The Lam–Teng pressure rises from 1.72845 to 6.91380 MPa for one to four layers; the ACI pressure rises from 1.5844125 to 6.33765 MPa. Domain decisions use full precision before display rounding.

Table 2(a). Model-specific pressures and confinement ratios for CFRP at 25 MPa

n	fl LT MPa	Ratio LT	fl ACI MPa	Ratio ACI	ACI ratio status
0	0.00000	0.000000	0.00000	0.000000	Control
1	1.72845	0.069138	1.58441	0.063377	Below 0.08 †
2	3.45690	0.138276	3.16883	0.126753	Ratio ≥ 0.08
3	5.18535	0.207414	4.75324	0.190130	Ratio ≥ 0.08
4	6.91380	0.276552	6.33765	0.253506	Ratio ≥ 0.08

Table 2(b). Strength and ideal section capacity indices for CFRP at 25 MPa

n	fcc LT MPa	Gain LT %	fcc ACI MPa	Gain ACI %	P0 LT kN	P0 ACI kN
0	25.0	0.0	25.0	0.0	3,312	3,312
1	25.0	0.0	30.0 †	19.9 †	3,312	3,836 †
2	36.4	45.6	34.9	39.7	4,515	4,359
3	42.1	68.4	39.9	59.6	5,116	4,883
4	47.8	91.3	44.9	79.5	5,718	5,407

† Below the ACI 0.08 ratio criterion. These values are algebraic evaluations, excluded from strengthening-capacity conclusions. P_0 is an ideal section index.

For one CFRP layer at 25 MPa, the Lam–Teng ratio is 0.069138 < 0.070000, so the adopted strength branch gives f'cc = 25.0 MPa. For two, three, and four layers, strengths are 36.4, 42.1, and 47.8 MPa and ideal P_0 values are 4,515, 5,116, and 5,718 kN. Relative to the 3,312 kN control, P_0 increases by 36.3%, 54.5%, and 72.6%. The steel contribution is unchanged, so the relative increase in P_0 is smaller than that in concrete strength.

The one-layer ACI ratio is 0.063377, below 0.08. The algebraic values 30.0 MPa and 3,836 kN are retained with a dagger in Table 2(b), but they do not support an ACI strengthening-capacity claim. Two to four layers pass the ratio criterion; their strengths are 34.9, 39.9, and 44.9 MPa, about 4.0%, 5.2%, and 6.2% below the corresponding Lam–Teng values. Figure 1 separates the one-layer algebraic ACI point from the line joining the ratio-qualified values.

This work is licensed under a Creative Commons Attribution 4.0 International license
Structures, Infrastructure, Planning, Implementation, and Legislation (SIPIL)
Vol. 2, No. 2, October 2026

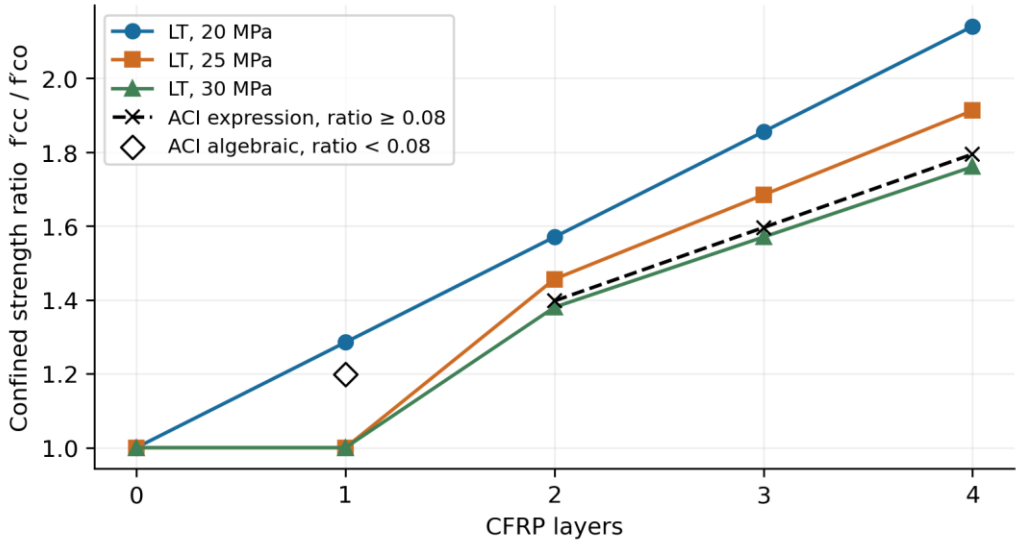


Figure 1. Calculated confined-strength ratios. The isolated open ACI point is below the 0.08 ratio criterion; the connected ACI points satisfy that criterion only. All values are analytical

2. Stress strain response and axial strain capacity

Figure 2 shows the adopted concrete stress–strain curves at 25 MPa. The separate control reaches its maximum stress at ε = 0.002 and is terminated at 0.003. Cases with $n \geq 2$ have a parabolic first branch followed by a linear hardening branch. The one-layer case has a flat second branch because its adopted strength gain is zero. The flat branch is a model idealization and should not be interpreted as measured low-confinement behavior.

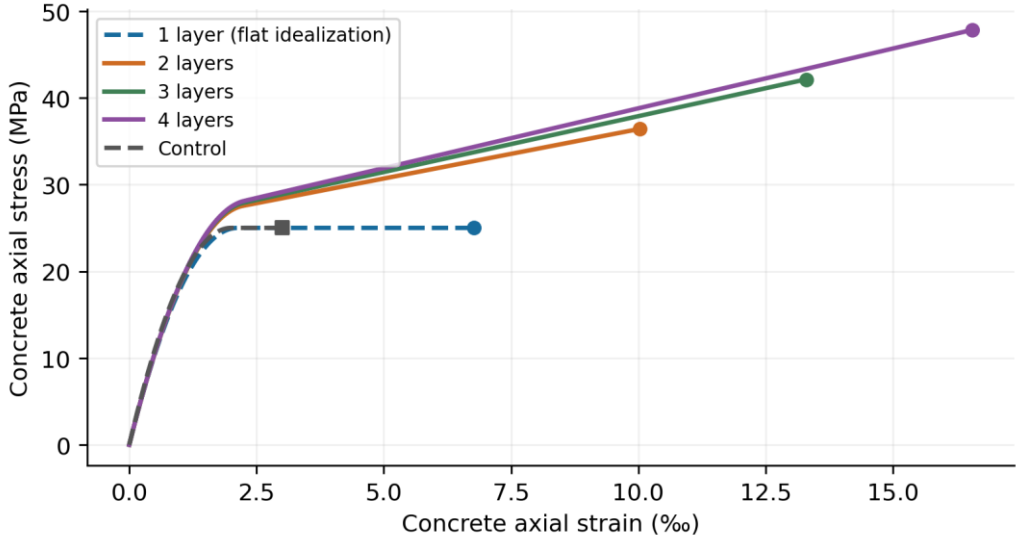


Figure 2. Calculated Lam–Teng concrete curves at 25 MPa. Dashed lines distinguish the separate control and the below-threshold one-layer idealization; symbols mark terminal points

Table 3 reports terminal axial strain, the axial strain index, and monotonic strain energy density. The Lam–Teng implementation gives 3.0‰ for the control, 6.8‰ for one layer, and 16.6‰ for four layers. The index $\varepsilon_{cu}/0.002$ rises from 1.5 to 8.3, and the energy density from 58 to 584 kJ/m^3. These are material-response measures. With the revised ACI peak-strain choice of 0.002, the two-layer value is

This work is licensed under a Creative Commons Attribution 4.0 International license

8.8‰; the three-layer value reaches 10.0‰ and the four-layer value remains at that cap. The one-layer ACI strain is an out-of-domain algebraic evaluation, not an accepted strengthening prediction.

Table 3. Terminal axial strain, axial strain index, and monotonic strain energy density for CFRP at 25 MPa

n	ε_{cu} L&T (‰)	Axial strain index εcu/0.002 (LT)	ε_{ccu} ACI (‰)	W LT kJ/m³	$W/W_{control}$
0	3.0	1.5	3.0	58	1.0
1	6.8	3.4	5.9 †	151	2.6
2	10.0	5.0	8.8	289	5.0
3	13.3	6.6	10.0	427	7.3
4	16.6	8.3	10.0	584	10.0

ACI strain uses ε'_c = 0.002. † Algebraic strain below the 0.08 ratio criterion. The 3.0‰ control is the separate unwrapped idealization.

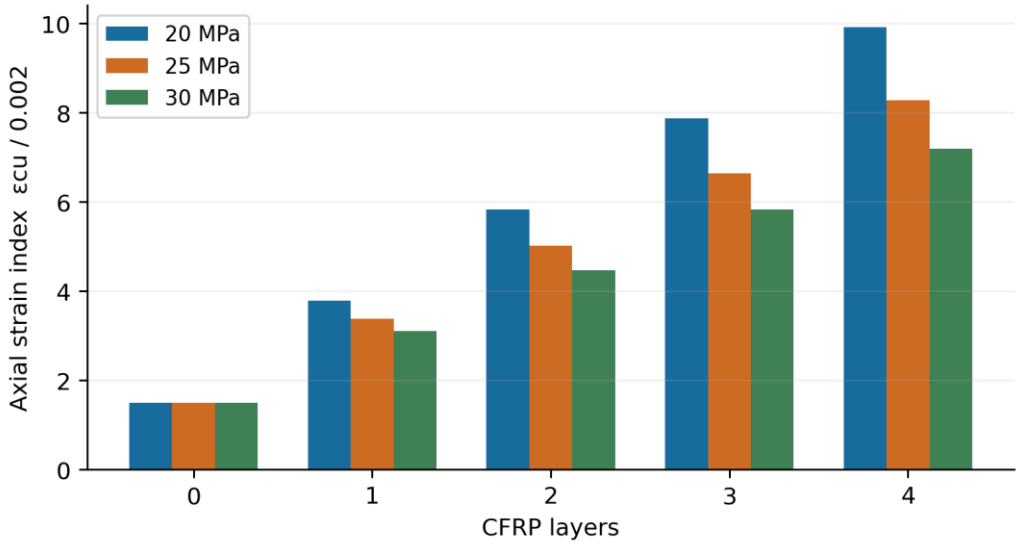


Figure 3. Calculated axial strain index $\varepsilon_{cu}/0.002$ for the adopted Lam–Teng implementation. This index is not member displacement ductility

3. Ideal section load strain response

Figure 4 superposes the concrete and steel responses. Steel yields at f_y/E_s = 0.00210. In the separate control, concrete has already reached its plateau at 0.002, and the section reaches 3,312 kN when the steel yields; 0.003 is the selected terminal strain, not the first occurrence of maximum load. The one-layer implementation also develops a load plateau. For n = 2–4, the hardening concrete branch raises the terminal load to 4,515, 5,116, and 5,718 kN at concrete axial strains of 10.0‰, 13.3‰, and 16.6‰. These axial terminal strains are not equal to the effective FRP hoop rupture strains.

This work is licensed under a Creative Commons Attribution 4.0 International license
Structures, Infrastructure, Planning, Implementation, and Legislation (SIPIL)
Vol. 2, No. 2, October 2026

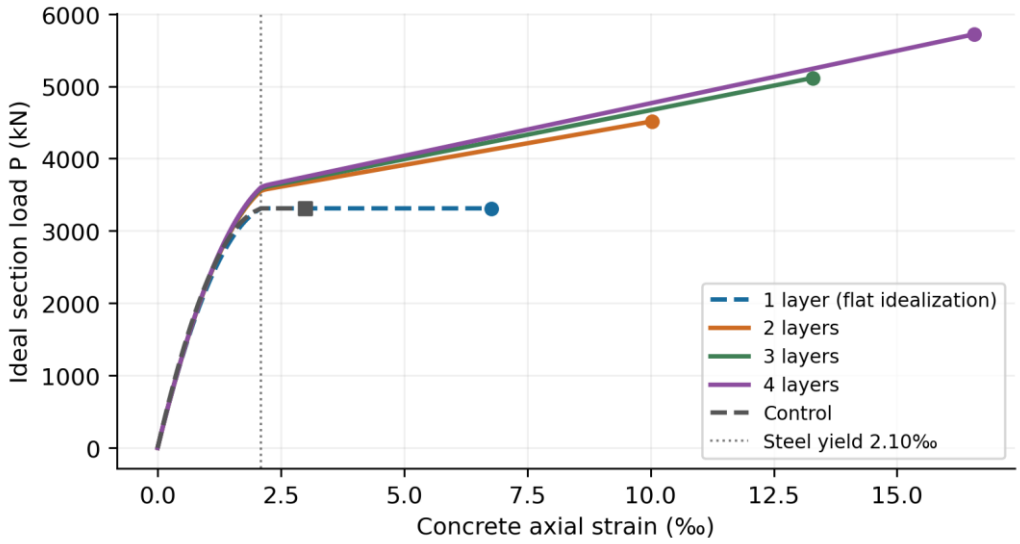


Figure 4. Calculated ideal section load–strain curves at 25 MPa. The vertical line marks steel yield at 2.10‰; symbols mark each terminal concrete axial strain

4. Concrete strength and assumed FRP system

Table 4 compares the three concrete strengths and the two fiber types for two and four layers, and Figure 5 shows the increase in axial capacity as a function of the number of layers. Lower-strength concrete benefited more. With four layers of CFRP, the confined strength gain was 114.1 %, 91.3 %, and 76.1 % for f'_{co} = 20, 25, and 30 MPa, and the corresponding increases in P_0 were 86.4 %, 72.6 %, and 62.7 %. This follows directly from Eq. (2): for the same confining pressure, the ratio f_l/f'_{co} is larger when f'_{co} is smaller.

Table 4. Lam–Teng predictions for the selected concrete strengths and assumed FRP systems

f'_{co} (MPa)	FRP	n	f_l (MPa)	f'_{cc} (MPa)	Gain (%)	ε_{cu} (‰)	Ideal P0 kN	P_0 gain (%)
20	CFRP	2	3.46	31.4	57.0	11.7	3,987	43.2
20	CFRP	4	6.91	42.8	114.1	19.8	5,190	86.4
20	GFRP	2	3.40	31.2	56.1	13.0	3,968	42.5
20	GFRP	4	6.80	42.4	112.2	22.6	5,152	85.0
25	CFRP	2	3.46	36.4	45.6	10.0	4,515	36.3
25	CFRP	4	6.91	47.8	91.3	16.6	5,718	72.6
25	GFRP	2	3.40	36.2	44.9	11.1	4,495	35.7
25	GFRP	4	6.80	47.4	89.8	18.8	5,679	71.5
30	CFRP	2	3.46	41.4	38.0	8.9	5,042	31.3
30	CFRP	4	6.91	52.8	76.1	14.4	6,245	62.7
30	GFRP	2	3.40	41.2	37.4	9.9	5,023	30.8

This work is licensed under a Creative Commons Attribution 4.0 International license

f'_{co} (MPa)	FRP	n	f_l (MPa)	f'_{cc} (MPa)	Gain (%)	ε_{cu} (‰)	Ideal P0 kN	P_0 gain (%)
30	GFRP	4	6.80	52.4	74.8	16.2	6,206	61.7

The near-equal confinement pressures were selected through the assumed inputs. For 25 MPa and four layers, strengths are 47.8 MPa for CFRP and 47.4 MPa for GFRP, while terminal strains are 16.5597‰ and 18.7675‰. The GFRP value is 13.33% higher when CFRP is the denominator. Across the two- and four-layer pairs in Table 4, the difference ranges from about 10.29% to 13.92%. Because membrane stiffness and rupture strain also differ, these results do not establish a general fiber-type effect or product interchangeability.

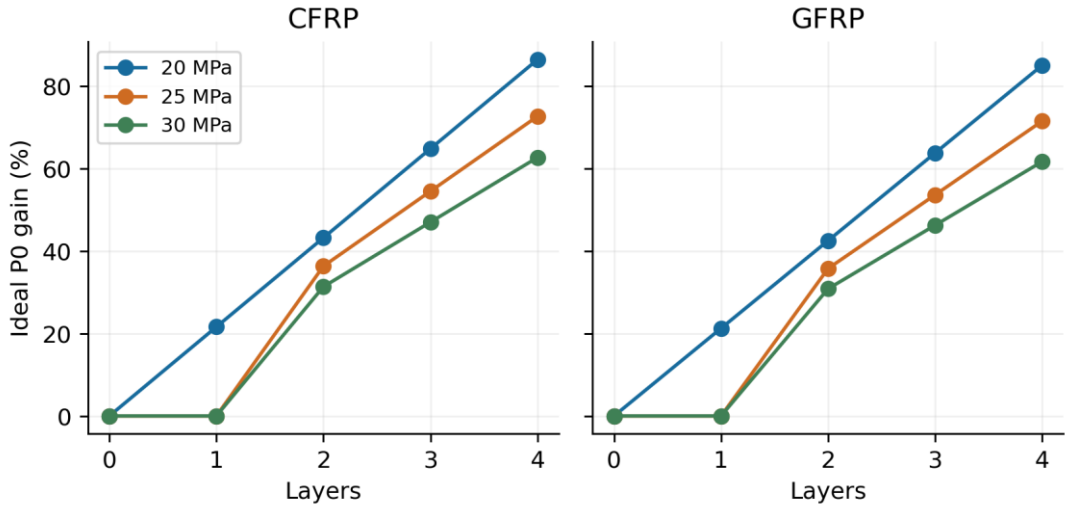


Figure 5. Calculated gains in ideal section capacity P_0 for the two assumed FRP systems using the adopted Lam–Teng implementation.

DISCUSSION

1. Strength and axial strain capacity

At 25 MPa, the adopted one-layer Lam–Teng branch gives no strength gain while its algebraic terminal axial strain exceeds that of the separately defined control. This illustrates a consequence of the selected equations, not proof that an actual insufficiently confined RC member is less brittle. Models for stress reduction and recovery are discussed by Liao et al. (2023), Shayanfar and Barros (2024), and Teng et al. (2009). Independent observations would be needed to assess whether the flat one-layer idealization is appropriate near the threshold.

The four-layer strain index is approximately 5.5 times the control index, and its monotonic energy density is about 10 times the control value. These increases do not establish lateral displacement ductility or hysteretic energy dissipation during earthquakes. Cyclic lateral loading, axial–flexural interaction, drift, stiffness degradation, and member failure mechanisms were not analyzed. PET and PEN systems discussed by Yuan, Bai, et al. (2022) and Yuan, Han, and Bai (2022) are outside the present input sets.

2. Domain checks and parameter sensitivity

Across all six one-layer combinations of concrete strength and assumed FRP system, the ACI ratios range from 0.051967 to 0.079221 and remain below 0.08. All two- to four-layer combinations

This work is licensed under a Creative Commons Attribution 4.0 International license

pass that ratio check. Therefore, a comparison of the one-layer ACI algebraic gain with the Lam–Teng zero-gain branch is not a comparison of two accepted strengthening predictions. At 25 MPa, both formulations give increasing strain from two to three layers, whereas the imposed ACI cap prevents a further strain increase at four layers. Lower calculated values alone do not establish conservatism or accuracy.

For the 25 MPa one-layer CFRP case, changing the assumed Lam–Teng efficiency from 0.55 to 0.60 and 0.65 gives confinement ratios of 0.063377, 0.069138, and 0.074900. The first two use the zero-strength-gain branch, while 0.65 gives a calculated strength of 31.18 MPa. The transition occurs at an efficiency of about 0.60748. These are deterministic scenarios around the adopted value, not statistical confidence bounds. They show why a rounded ratio of 0.07 is unsuitable for choosing the strength branch.

3. Practical implications

For CFRP at 25 MPa, the two-, three-, and four-layer ideal capacities increase by about 601.46 kN per added layer after $n = 2$. Dividing their percentage gains by total layer count gives essentially the same value, about 18.16 percentage points per layer. No cost function, target reliability, or economic optimization was included, so an optimum of two to three layers cannot be inferred. A minimum count satisfying a confinement ratio is distinct from a count that meets a complete member design target. Comparing product substitutions also requires consistent material qualification and durability evidence.

Future experimental assessment should target the threshold region, vary confinement stiffness as well as rupture strain, and use measured material properties. Tests at more than one diameter and concrete strength would help determine whether the numerical trends extend beyond the assumed 400 mm section. Such tests are proposed work; no additional experimental results are presented here.

4. Limitations

The results are deterministic outputs for assumed inputs. No laboratory tests or independent experimental benchmark are included. The model addresses uniform concentric compression of a circular section and omits member stability, eccentricity, bar buckling, cover loss, transverse-steel interaction, overlap failure, environmental deterioration, and time-dependent effects. The selected FRP systems have similar pressures but different stiffnesses. The low-confinement flat branch and separate control law affect the strain and energy comparisons. Near the threshold, modest changes in assumed efficiency can change the strength branch. ACI labels report only the ratio criterion examined here. Neither formulation is shown to be accurate or conservative by the present calculation alone.

CONCLUSIONS

The analytical comparison of a 400 mm circular RC section gives the following conditional findings:

1. For 25 MPa and two to four CFRP layers, the adopted Lam–Teng implementation gives concrete-strength gains of 45.6–91.3% and ideal section-capacity gains of 36.3–72.6%. The axial strain index rises from 1.5 for the separate control to 5.0–8.3; these indices are not seismic displacement ductilities.
2. For the assumed 25 MPa one-layer CFRP case, the Lam–Teng ratio 0.069138 is below 0.07. The adopted branch gives no strength gain and a larger algebraic terminal axial strain. Actual low-confinement behavior requires independent validation.

This work is licensed under a Creative Commons Attribution 4.0 International license

3. For the selected four-layer CFRP input, ideal capacity gains are 86.4%, 72.6%, and 62.7% at 20, 25, and 30 MPa. This trend follows from the assumed equal pressure at different concrete strengths.
4. For the matched 25 MPa four-layer input systems, the predicted GFRP terminal axial strain is 13.33% greater than CFRP. This is conditional on the chosen stiffnesses, thicknesses, and rupture strains and does not show general product equivalence.
5. All six one-layer ACI combinations are below the 0.08 ratio criterion and are reported only as algebraic evaluations. At 25 MPa, the ratio-qualified two- to four-layer ACI strengths are 4.0–6.2% below the corresponding Lam–Teng strengths. With ε'_c = 0.002, strain increases from 8.8‰ at two layers to 10.0‰ at three layers, with no further increase at four layers.
6. The calculations do not establish cyclic seismic performance, an economic optimum, or a complete strengthening design. Independent benchmarking and qualified product data are required before drawing those conclusions.

REFERENCES

American Concrete Institute. (2017). Guide for the design and construction of externally bonded FRP systems for strengthening concrete structures (ACI 440.2R-17). American Concrete Institute.

Badan Standardisasi Nasional. (2019). Persyaratan beton struktural untuk bangunan gedung (SNI 2847:2019). Badan Standardisasi Nasional.

Cao, Y., Zhao, G., Zhang, Y., Hou, C., & Mao, L. (2022). Unified stress–strain model of FRP-confined square and circle rubber concrete columns. Materials, 15(5), Article 1832. https://doi.org/10.3390/ma15051832

Chaallal, O., Hassan, M., & LeBlanc, M. (2006). Circular columns confined with FRP: Experimental versus predictions of models and guidelines. Journal of Composites for Construction, 10(1), 4–12. https://doi.org/10.1061/(ASCE)1090-0268(2006)10:1(4)

Chen, G.-M., Lan, Z.-H., Xiong, M.-X., & Xu, Z. (2020). Compressive behavior of FRP-confined steel-reinforced high strength concrete columns. Engineering Structures, 220, Article 110990. https://doi.org/10.1016/j.engstruct.2020.110990

Debaiky, A. S., Green, M. F., & Hope, B. B. (2007). Modeling of corroded FRP-wrapped reinforced concrete columns in axial compression. Journal of Composites for Construction, 11(6), 556–564. https://doi.org/10.1061/(ASCE)1090-0268(2007)11:6(556)

Hu, H., & Seracino, R. (2014). Analytical model for FRP-and-steel-confined circular concrete columns in compression. Journal of Composites for Construction, 18(3), Article 04013048. https://doi.org/10.1061/(ASCE)CC.1943-5614.0000394

Hu, Z., Li, Q., Yan, H., & Wen, Y. (2021). Experimental study on slender CFRP-confined circular RC columns under axial compression. Applied Sciences, 11(9), Article 3968. https://doi.org/10.3390/app11093968

Jamatia, R., & Deb, A. (2017). Size effect in FRP-confined concrete under axial compression. Journal of Composites for Construction, 21(6), Article 04017047. https://doi.org/10.1061/(ASCE)CC.1943-5614.0000825

Lam, L., & Teng, J. G. (2003). Design-oriented stress–strain model for FRP-confined concrete. Construction and Building Materials, 17(6–7), 471–489. https://doi.org/10.1016/S0950-0618(03)00045-X

This work is licensed under a Creative Commons Attribution 4.0 International license

Lee, C.-S., & Hegemier, G. A. (2009). Model of FRP-confined concrete cylinders in axial compression. Journal of Composites for Construction, 13(5), 442–454. https://doi.org/10.1061/(ASCE)CC.1943-5614.0000029

Liao, J., Zeng, J.-J., Zhuge, Y., Zheng, Y., Ma, G., & Zhang, L. (2023). FRP-confined concrete columns with a stress reduction–recovery behavior: A state-of-the-art review, design recommendations and model assessments. Composite Structures, 321, Article 117313. https://doi.org/10.1016/j.compstruct.2023.117313

Nematzadeh, M., Mousavimehr, M., Shayanfar, J., & Omidalizadeh, M. (2021). Eccentric compressive behavior of steel fiber-reinforced RC columns strengthened with CFRP wraps: Experimental investigation and analytical modeling. Engineering Structures, 226, Article 111389. https://doi.org/10.1016/j.engstruct.2020.111389

Ozbakkaloglu, T., & Lim, J. C. (2013). Axial compressive behavior of FRP-confined concrete: Experimental test database and a new design-oriented model. Composites Part B: Engineering, 55, 607–634. https://doi.org/10.1016/j.compositesb.2013.07.025

Ozbakkaloglu, T., Lim, J. C., & Vincent, T. (2013). FRP-confined concrete in circular sections: Review and assessment of stress–strain models. Engineering Structures, 49, 1068–1088. https://doi.org/10.1016/j.engstruct.2012.06.010

Shayanfar, J., & Barros, J. A. O. (2024). Design-oriented model of unified character to determine softening–hardening stress–strain behavior of FRP-confined concrete columns of general cross section. Journal of Composites for Construction, 28(6), Article 04024059. https://doi.org/10.1061/JCCOF2.CCENG-4772

Shayanfar, J., Barros, J. A. O., Abedi, M., & Rezazadeh, M. (2023). Unified compressive strength and strain ductility models for fully and partially FRP-confined circular, square, and rectangular concrete columns. Journal of Composites for Construction, 27(6), Article 04023053. https://doi.org/10.1061/JCCOF2.CCENG-4336

Shayanfar, J., Barros, J. A. O., & Pereira, J. P. C. A. (2024). A versatile model with a design framework for axially-loaded FRP-confined concrete with/without a stress reduction–recovery behavior. Construction and Building Materials, 448, Article 138097. https://doi.org/10.1016/j.conbuildmat.2024.138097

Shayanfar, J., Barros, J. A. O., & Rezazadeh, M. (2022). Unified model for fully and partially FRP-confined circular and square concrete columns subjected to axial compression. Engineering Structures, 251, Article 113355. https://doi.org/10.1016/j.engstruct.2021.113355

Shayanfar, J., Barros, J. A. O., & Rezazadeh, M. (2023). Cross-sectional and confining system unification on peak compressive strength of FRP-confined concrete. Structural Concrete, 24(1), 1531–1545. https://doi.org/10.1002/suco.202200105

Shayanfar, J., Barros, J. A. O., & Rezazadeh, M. (2020). Analytical model to predict dilation behavior of FRP-confined circular concrete columns subjected to axial compressive loading. Journal of Composites for Construction, 24(6), Article 04020071. https://doi.org/10.1061/(ASCE)CC.1943-5614.0001087

Shayanfar, J., Barros, J. A. O., Rezazadeh, M., & Kafshgarkolaei, H. J. (2025). Enhancing the performance of heat-damaged rectangular RC columns using prestressed FRP confinement. Construction and Building Materials, 501, Article 144346. https://doi.org/10.1016/j.conbuildmat.2025.144346

This work is licensed under a Creative Commons Attribution 4.0 International license

Shayanfar, J., Pereira, J. P. C. A., & Barros, J. A. O. (2025). Passive confinement scenarios for strengthening fire-damaged concrete columns: Experimental and analytical research. Structures, 73, Article 108375. https://doi.org/10.1016/j.istruc.2025.108375

Silva Lobo, P., Faustino, P., Jesus, M., & Marreiros, R. (2018). Design model of concrete for circular columns confined with AFRP. Composite Structures, 200, 69–78. https://doi.org/10.1016/j.compstruct.2018.05.094

Spoelstra, M. R., & Monti, G. (1999). FRP-confined concrete model. Journal of Composites for Construction, 3(3), 143–150. https://doi.org/10.1061/(ASCE)1090-0268(1999)3:3(143)

Teng, J. G., Jiang, T., Lam, L., & Luo, Y. Z. (2009). Refinement of a design-oriented stress–strain model for FRP-confined concrete. Journal of Composites for Construction, 13(4), 269–278. https://doi.org/10.1061/(ASCE)CC.1943-5614.0000012

Thériault, M., Neale, K. W., & Claude, S. (2004). Fiber-reinforced polymer-confined circular concrete columns: Investigation of size and slenderness effects. Journal of Composites for Construction, 8(4), 323–331. https://doi.org/10.1061/(ASCE)1090-0268(2004)8:4(323)

Yuan, W.-Y., Bai, Y.-L., Han, Q., & Zhang, S.-M. (2022). Large rupture strain FRP-confined concrete columns of different sizes: Experiments and stress–strain models. Journal of Composites for Construction, 26(4), Article 04022040. https://doi.org/10.1061/(ASCE)CC.1943-5614.0001229

Yuan, W.-Y., Han, Q., & Bai, Y.-L. (2022). A unified stress–strain model for LRS FRP-confined concrete columns with square and circular cross-sections. Engineering Structures, 255, Article 113900. https://doi.org/10.1016/j.engstruct.2022.113900